

Minimum Covariance Determinant: Spectral Embedding and Subset Size Determination

Qiang Heng*, Hui Shen[†], Kenneth Lange[‡]

Abstract

This paper introduces several enhancements to the minimum covariance determinant method of outlier detection and robust estimation of means and covariances. We leverage the principal component transform to achieve dimension reduction and ultimately better analyses. Our best subset selection algorithm strategically combines statistical depth and concentration steps. To ascertain the appropriate subset size and number of principal components, we introduce a bootstrap procedure that estimates the instability of the best subset algorithm. The parameter combination exhibiting minimal instability proves ideal for the purposes of outlier detection and robust estimation. Rigorous benchmarking against prominent MCD variants showcases our approach's superior statistical performance and computational speed in high dimensions. Application to a fruit spectra data set and a cancer genomics data set illustrates our claims.

Keywords: Robustness, Outliers, Principal component analysis, Statistical depth, Bootstrap, Algorithm instability, High-dimensional data, Model selection

1 Introduction

The minimum covariance determinant (MCD) estimator ([Rousseeuw, 1985](#)) and its subsequent extensions have been widely adopted for robust estimation of multivariate location and scatter. This estimator identifies a subset of a predetermined size from an $n \times p$ multivariate data matrix, aiming for the smallest possible determinant of the reduced sample

*Department of Computational Medicine, UCLA

[†]Department of Mathematics and Statistics, McGill University

[‡]Departments of Computational Medicine, Human Genetics, and Statistics, UCLA

covariance matrix. MCD rose in popularity after the introduction of a computationally efficient algorithm called fast minimum covariance determinant (FastMCD) (Rousseeuw and Driessen, 1999). FastMCD has found broad applications in finance, econometrics, engineering, the physical sciences, and biomedical research (Hubert et al., 2008, 2018). The minimum covariance determinant estimator is statistically consistent and asymptotically normal (Butler et al., 1993; Cator and Lopuhaä, 2012). Recent extensions to the MCD paradigm include a kernelized version (Schreurs et al., 2021) for nonelliptical data and a cell-wise version (Raymaekers and Rousseeuw, 2023) for robustness against cell-wise outliers.

In the univariate case (Rousseeuw and Leroy, 2005), the MCD problem can be exactly solved in $O(n \log n)$ arithmetic operations. Unfortunately, computation becomes much more challenging in the multivariate setting. FastMCD is essentially a greedy block minimization algorithm, providing a locally optimal solution for the nonconvex, combinatorial optimization problem of minimizing the subsample covariance determinant. Given its greedy nature, the block-descent algorithm can be trapped by local minima. Therefore, proper initialization is crucial, particularly as the proportion of outliers or the dimensionality of the data grows. Naive random initialization falters in these circumstances. Hubert et al. (2012) propose a deterministic initialization strategy called deterministic minimum covariance determinant (DetMCD) that relies on six different initializations for μ and Σ . This ensemble strategy can substantially outperform random initialization in robustness and speed when the proportion of outliers is high. However, recent work by Zhang et al. (2023) demonstrates that using the trimmed subset induced by the notion of projection depth (Zuo and Serfling, 2000) is conceptually simpler, computationally faster, and even more robust.

To its detriment, MCD relies on the computation of Mahalanobis distances, which requires the invertibility of $\hat{\Sigma}$. To tackle the high-dimensional scenario $p > n$, Boudt et al. (2020) add Tikhonov regularization to the covariance matrix to ensure its positive definiteness. However, their minimum regularized covariance determinant (MRCD) estimator is computationally expensive due to its need to invert large matrices at each iteration. Other tactics for high-dimensional outlier detection rely on alternative definitions of Mahalanobis distance and formulate the problem in the framework of hypothesis testing. For example, Ro et al. (2015), Li and Jin (2022), and Li et al. (2024) study the null asymptotic distribution in this context under suitable model assumptions.

This paper explores several new ideas for enhancing and expanding algorithms for the MCD problem. We first propose best subset selection based on spectral embedding and statistical depth. The use of principal components for dimension reduction in outlier detection was previously explored by [Hubert et al. \(2005\)](#), [Filzmoser et al. \(2008\)](#), and [Zahariah and Midi \(2023\)](#). Compared with these existing approaches, our algorithm does not require a robust estimate of covariance matrices. We demonstrate that ordinary PCA is sufficient for revealing inlier/outlier structure and that outlier detection can be performed after spectral embedding. Our second major contribution is the construction of a bootstrap procedure for simultaneously estimating the number of inliers h and the appropriate number of principal components q . The current literature largely ignores principled ways of selecting h . Often h is chosen conservatively to ensure the exclusion of every conceivable outlier from the selected subset. Popular choices include $h = \lfloor 0.5n \rfloor$ and $h = \lfloor 0.75n \rfloor$. These arbitrary choices potentially compromise statistical efficiency. Although various reweighting procedures ([Rousseeuw and Driessen, 1999](#); [Hardin and Roche, 2005](#); [Cerioli, 2010](#); [Ro et al., 2015](#); [Li et al., 2024](#)) can be applied to rescue additional observations as inliers ([Rousseeuw and Driessen, 1999](#)), such reweighting procedures requires the specification of a significance level that balances type-I error and power. Selecting the appropriate significance level or cut-off threshold raises a barrier to model selection. When model assumptions are not met, the performance of reweighting procedures may also severely deteriorate due to their parametric nature. In a manner akin to *clustering instability* ([Wang, 2010](#); [Fang and Wang, 2012](#)), our bootstrap procedure estimates the instability of our h -subset selection algorithm. We find that the subset size exhibiting minimal instability almost always matches the true number of inliers. Thus, the estimated h enables us to incorporate as many observations as possible in estimating means and covariances. In short, the selected h -subset helps discriminate between outliers and inliers in a data-driven, nonparametric, robust manner and eliminates the need for a pre-defined significance level.

2 Background

2.1 Minimum Covariance Determinant

Given a multivariate data matrix $X \in \mathbb{R}^{n \times p}$, assume that most of the observations are sampled from a unimodal distribution with mean $\mu \in \mathbb{R}^p$ and covariance $\Sigma \in \mathbb{R}^{p \times p}$.

Simultaneously suppose that there exists a subset of outliers markedly diverging from the primary mode. For the purpose of outlier detection and robust estimation, we are interested in finding a subset $H \subset \{1, 2, \dots, n\}$ of size h that is outlier-free. The mean and covariance estimated from the subset are given by

$$\hat{\mu} = \frac{1}{h} \sum_{i \in H} x_i \quad \text{and} \quad \hat{\Sigma} = \frac{1}{h} \sum_{i \in H} (x_i - \hat{\mu})(x_i - \hat{\mu})^\top, \quad (1)$$

where the $x_i \in \mathbb{R}^p$ are the rows of X indexed by the integer subset H .

Definition 2.1. *The minimum covariance determinant problem seeks the h observations from x_1, x_2, \dots, x_n minimizing the determinant of $\hat{\Sigma}$ defined in equation (1).*

Rousseeuw and Driessen (1999) proposed the first computationally efficient algorithm (FastMCD) to tackle the MCD problem. Starting from a random initial subset H , FastMCD first obtains an initial estimate of μ and Σ via equation (1). Then, based on the Mahalanobis distances

$$d_i = \sqrt{(x_i - \hat{\mu})^\top \hat{\Sigma}^{-1} (x_i - \hat{\mu})}, \quad (2)$$

the observations $x_i, i = 1, 2, \dots, n$ are ranked from closest to furthest. Given the permutation π producing the ranking $d_{\pi(1)} \leq d_{\pi(2)} \leq \dots \leq d_{\pi(n)}$, H is updated as

$$H = \{\pi(1), \pi(2), \dots, \pi(h)\}. \quad (3)$$

Rousseeuw and Driessen (1999) call the combination of procedures (1), (2), and (3) a concentration step (C-step). Invoking a uniqueness property (Grübel, 1988), Rousseeuw and Driessen (1999) show that each concentration step monotonically decreases $\det(\hat{\Sigma})$. We demonstrate that the minimum covariance determinant problem as defined in Definition 2.1 is, in fact, equivalent to a subsample likelihood maximization problem.

Proposition 2.1. *The minimum covariance determinant problem is equivalent to*

$$\begin{aligned} & \underset{w \in \mathbb{R}^n, \mu, \Sigma > 0}{\text{minimize}} && \sum_{i=1}^n w_i [\log\{\det(\Sigma)\} + (x_i - \mu)^\top \Sigma^{-1} (x_i - \mu)] \\ & \text{such that} && \sum_{i=1}^n w_i = h, \quad w_i \in \{0, 1\}. \end{aligned} \quad (4)$$

The descent property of the concentration step is a natural corollary of this interpretation. Thus, we provide an alternative proof of the descent property that is more intuitive.

Corollary 2.1. *Iteratively applying (1), (2), and (3) monotonically decreases $\det \hat{\Sigma}$.*

2.2 Statistical Depth

Statistical depth is a nonparametric notion commonly used to rank multivariate data from a center outward (Zuo and Serfling, 2000; Zhang et al., 2023). A statistical depth function increases with the centrality of the observation, with values ranging between 0 and 1. After computing the statistical depth of all observations within a data set, it is natural in estimating means and covariances to retain the h observations with the greatest depths. Zhang et al. (2023) investigated the application of two representative depth notions, projection depth and L_2 depth (Zuo and Serfling, 2000). Their experiments demonstrate that projection depth is more robust across different simulation settings. Projection depth has the added benefit of being affine invariant (Zuo and Serfling, 2000; Zuo, 2006). Therefore, we focus on projection depth as our primary depth notion.

Definition 2.2. *The projection depth of a vector $x \in \mathbb{R}^p$ with respect to a distribution F is defined as*

$$D(x; F) = \left[1 + \sup_{\|u\|=1} \frac{|u^\top x - \text{med}(u^\top y)|}{\text{MAD}(u^\top y)} \right]^{-1}, \quad (5)$$

where y is a multivariate random variable that follows the distribution F , $\text{med}(V)$ is the median of a univariate random variable V , and $\text{MAD}(V) = \text{med}(|V - \text{med}(V)|)$ is the median absolute deviation from the median.

Since there exists no closed-form expression for the quantity (5), in practise projection depth is approximated by generating k random directions u . For the purpose of ranking the observations from a center outward, one can compute $D(x_i; \hat{F}_n)$ for i between 1 and n , where \hat{F}_n is the empirical distribution of $X \in \mathbb{R}^{n \times p}$. In this case projection depth is also referred to as sample projection depth. We may write $D(x_i; \hat{F}_n)$ as $D(x_i; X)$ to highlight its dependence on the observed data matrix X . Sample projection depths are generally efficient to compute with a time complexity of $O(nkp)$. In the R computing environment, the package `ddalpha` (Lange et al., 2014; Pokotylo et al., 2016) efficiently delivers sample projection depths.

2.3 Reweighted Estimators

Many MCD algorithms employ reweighting to avoid excluding too many observations. For example, the fast depth-based (FDB) algorithm of [Zhang et al. \(2023\)](#) consists of three steps: (a) compute statistical depths and define the initial h -subset to be the h observations with the largest depths (b) compute $\hat{\mu}$ and $\hat{\Sigma}$ by equation (1), and (c) re-estimate $\hat{\mu}$ and $\hat{\Sigma}$ via the reweighting scheme (6) of [Rousseeuw and Driessen \(1999\)](#). In summary,

$$c = \operatorname{med}_i \frac{\mathcal{D}^2(x_i; \hat{\mu}, \hat{\Sigma})}{\chi_{p,0.5}^2}, \quad w_i = \begin{cases} 1 & \mathcal{D}^2(x_i; \hat{\mu}, c\hat{\Sigma}) \leq \chi_{p,0.975}^2 \\ 0 & \mathcal{D}^2(x_i; \hat{\mu}, c\hat{\Sigma}) > \chi_{p,0.975}^2, \end{cases} \quad (6)$$

$$\hat{\mu}_{\text{re}} = \frac{\sum_{i=1}^n w_i x_i}{\sum_{i=1}^n w_i}, \quad \hat{\Sigma}_{\text{re}} = \frac{\sum_{i=1}^n w_i (x_i - \hat{\mu}_{\text{re}})(x_i - \hat{\mu}_{\text{re}})^\top}{\sum_{i=1}^n w_i - 1}.$$

Here $\mathcal{D}(x_i; \hat{\mu}, \hat{\Sigma})$ is the Mahalanobis distance of x_i from the center $\hat{\mu}$. FDB amends the depth-induced h -subset to include observations with weight 1 and skips concentration steps altogether. As we demonstrate in [Section 3.3](#) and [Section 5.1](#), a reweighting procedure like (6) can severely underestimate or overestimate the number of outliers.

3 Methods

3.1 Spectral Embedding

A key ingredient of our attack on MCD is to transform the data to its principal component scores before best subset selection. We first center the data matrix $X \in \mathbb{R}^{n \times p}$ and then compute the singular value decomposition $\tilde{X} = USV^T$ of the centered data \tilde{X} , where $V \in \mathbb{R}^{p \times \min\{n,p\}}$, and S has diagonal entries in decreasing order. Finally we select the first q principal components $Z = \tilde{X}V[:, 1 : q]$. The matrix Z is the substrate from which we identify the best h -subset.

Definition 3.1. *Suppose that the first q principal components of $X \in \mathbb{R}^{n \times p}$ is $Z \in \mathbb{R}^{n \times q}$. The spectral minimum covariance determinant problem with parameter q and h is the minimum covariance determinant problem with subset size h defined on Z .*

Proposition 3.1. *The spectral minimum covariance determinant problem is equivalent to the minimum covariance determinant problem when the number of principal components*

q is equal to the number of features p . Additionally, spectral MCD is location invariant and permutation invariant in this setting.

[Proposition 3.1](#) implies that the spectral minimum covariance determinant problem includes the MCD problem as a special case. If we properly choose the number of principal components, then SpectralMCD should be at least as powerful as MCD in outlier detection. Fortunately, we demonstrate that a good choice can be achieved via algorithm instability as introduced in [Section 3.3](#). It is also common practise to normalize the variables of the data matrix to have unit variance before performing principal component analysis. This action also makes our definition of the SpectralMCD scale invariant. However, we find empirically that rescaling is unnecessary to the purpose of outlier detection. Therefore for the sake of simplicity we choose to omit normalization in SpectralMCD.

The more interesting case is perhaps when the number of principal components q satisfies $q < p$. As noted in [Section 2.2](#), the time complexity for computing sample projection depths for a data set of size $n \times p$ is $O(nkp)$. Spectral embedding automatically alleviates the computational burden in estimating projection depth by reducing p to q . Spectral embedding may also reduce the required number of random directions k . The artificial ‘‘point’’ outlier data of ([Hubert et al., 2012](#); [Zhang et al., 2023](#)) illustrates the virtues of operating on principal component scores. [Section 4.1](#) outlines the protocol for generating these data. The data matrix X is 400×40 , with 25% of the observations replaced by outliers. [Figure 1](#) depicts the decline in the outlier count in the $h = 300$ retained observations as a function of k and q . As expected, with rising k , the h -subset includes fewer outliers. Employing only 2 or 10 principal components results in a notably faster decline in the average number of outliers compared to employing all 40 principal components. The left panel of [Figure 1](#) suggests that the first two principal components already capture the inlier/outlier structure. Because projection depth is affine invariant, using all 40 principal components for computing projection depths is equivalent to using the original data matrix X .

Our next proposition sheds light on the fact that similar to the standard MCD problem, SpectralMCD separates outliers from inliers with a quadratic form. However, the quadratic matrix A is likely singular, which facilitates dimension reduction.

Proposition 3.2. *The SpectralMCD subset H of X is separated from the rest of the data by a quadratic discriminant function. In other words, there exists $f(x) = x^\top Ax + b^\top x + c$,*

such that

$$\begin{aligned} f(x_i) &\leq 0, & \forall i \in H, \\ f(x_i) &\geq 0, & \forall i \notin H. \end{aligned}$$

Here A is positive semidefinite, but not necessarily positive definite.

It may be possible to deduce the asymptotic properties of SpectralMCD through the principal component matrix V . We conjecture that further study will lead to conclusions similar to those reached by [Butler et al. \(1993\)](#). For the sake of brevity, we defer this open problem to future investigation.

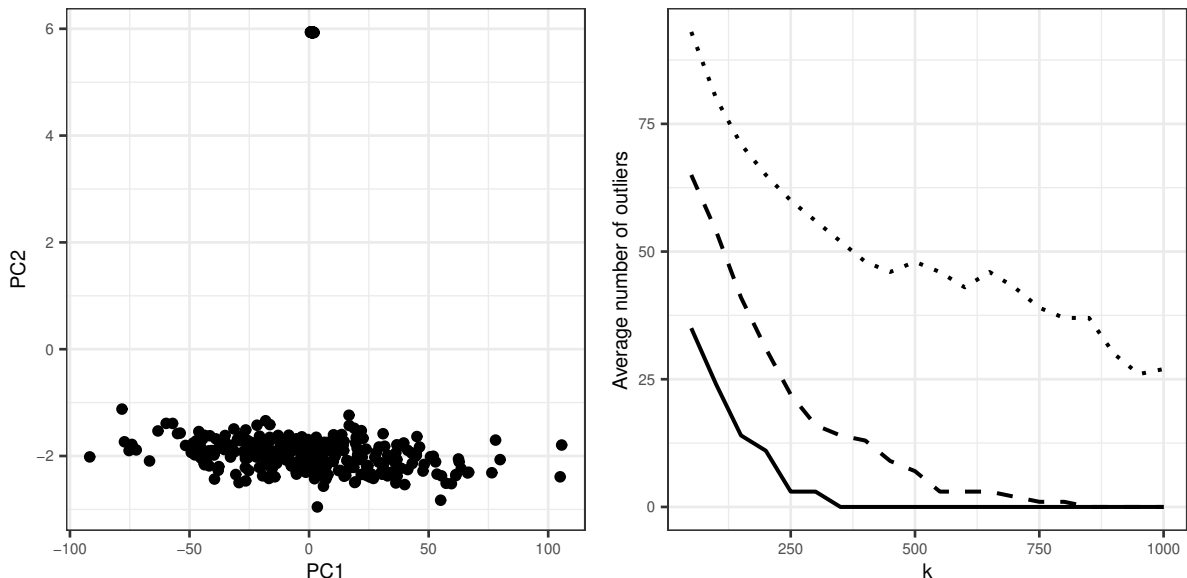


Figure 1: The left panel shows the distribution of the first and second principal components. The right panel shows the average number of outliers included in the h -subset induced by projection depths over 100 random replicates. Solid line shows counts for $q = 2$, dashed line shows counts for $q = 10$, and dotted line shows counts for $q = 40$.

3.2 Concentration Steps

When the specified subset size h is close to the true number of inliers and projection depth is difficult to approximate, [Figure 1](#) shows that depth-induced h -subsets may still contain several outliers. The FDB algorithm of [Zhang et al. \(2023\)](#), which skips concentration steps, is able to work well despite possible outliers in the initial h -subset because the reweighting step [\(6\)](#) adds an additional layer of projection. Unfortunately, we demonstrate in [Section 3.3](#) and [Section 5.1](#) that the reweighting step [\(6\)](#) itself may be

detrimental to outlier detection. Moreover, when $p > n$, the reweighting step is stymied by the singularity of the matrix $\hat{\Sigma}$. To ensure that the identified h -subset contains as few outliers as possible, we employ concentration steps as described in [Section 2.1](#) to further refine the h -subset. [Algorithm 1](#) summarizes our best h -subset selection algorithm.

Algorithm 1 Spectral Minimum Covariance Determinant (SpectralMCD)

Input: Data matrix $X \in \mathbb{R}^{n \times p}$, subset size $h < n$, number of principal components $q \leq \min\{n, p\}$, number of random directions k .

- 1: Center X to obtain \tilde{X} and compute the singular value decomposition $\tilde{X} = USV^T$.
- 2: Compute the principal components matrix $Z = \tilde{X}V[:, 1 : q]$ and the projection depths $d_i = D(z_i; Z), i = 1, 2, \dots, n$, using k random directions.
- 3: Sort d_i in decreasing order, yielding permutation π with $d_{\pi(1)} \geq d_{\pi(2)} \geq \dots \geq d_{\pi(n)}$. Set $H = \{\pi(1), \pi(2), \dots, \pi(h)\}$.
- 4: Update H using regular concentration steps (1), (2), and (3) on the principal component matrix Z until H stabilizes.

Output: The best h -subset H .

3.3 Estimating the Number of Outliers

In the MCD literature, selecting the right subset size h has posed a consistent challenge. Although spectral embedding brings numerous advantages, determining the optimal number of principal components remains a hurdle. A recent work proposed to use normality based test statistic to determine the subset size in a related but different problem of least trimmed squares ([Berenguer-Rico et al., 2023](#)). However, to our knowledge, there are very few options for determining the appropriate subset size in the MCD problem other than reweighting. Drawing inspiration from the notion of *clustering instability* ([Wang, 2010](#); [Fang and Wang, 2012](#)), we now describe a bootstrap procedure for estimating both the number of inliers h (equivalently the number of outliers $n - h$) and the appropriate number of principal components q . The task of robust location/scatter estimation can be viewed as a special case of clustering with two clusters, with one cluster consisting of inliers, and the other cluster consisting of outliers. Unlike traditional clustering, the outlier cluster does not necessarily exhibit spatial structure. This spatial ambiguity causes classic strategies in clustering, such as the gap statistic ([Tibshirani et al., 2001](#)), to fail. If the number of inliers h is suitably chosen, then different bootstrapped samples should yield similar conclusions about which cases are outliers in the data matrix X . Suppose the bootstrapped samples \dot{X} and \ddot{X} deliver indicator functions (binary maps) ψ_1 and ψ_2 distinguishing outliers from inliers, with a value of 1 denoting an outlier and a value

of 0 denoting an inlier. To measure the distance between ψ_1 and ψ_2 , we resort to the probability that ψ_1 and ψ_2 do not agree on an observation randomly selected from X .

Definition 3.2. *The probability distance between two binary maps ψ_1 and ψ_2 on a data matrix X is*

$$p_X(\psi_1, \psi_2) = \frac{1}{n} \sum_{i=1}^n |\psi_1(x_i) - \psi_2(x_i)|. \quad (7)$$

The distance $p_X(\psi_1, \psi_2)$ can be interpreted as the probability of the symmetric difference of the two outlier sets encoded by the binary maps. The following standard definition of clustering instability Wang (2010) allows for $K > 2$ clusters.

Definition 3.3. *The clustering distance between two clusterings ψ_1 and ψ_2 on the data matrix X is*

$$d_X(\psi_1, \psi_2) = \frac{1}{n^2} \sum_{i=1}^n \sum_{j=1}^n |I_{\psi_1(x_i)=\psi_1(x_j)} - I_{\psi_2(x_i)=\psi_2(x_j)}|, \quad (8)$$

where ψ_1 and ψ_2 map an arbitrary vector $x \in \mathbb{R}^p$ to a cluster label $k \in \{0, 1, \dots, K-1\}$.

The next proposition elucidates the connection between probability distance and clustering distance given just two clusters.

Proposition 3.3. *When there is only two clusters ($K = 2$), the two distances covered by Definition 3.2 and Definition 3.3 satisfy*

$$d_X(\psi_1, \psi_2) = 2p_X(\psi_1, \psi_2)[1 - p_X(\psi_1, \psi_2)].$$

Proposition 3.3 reduces the computational complexity of computing $d_X(\psi_1, \psi_2)$ from $O(n^2)$ to $O(n)$. This saves computation time when n is large.

Haslbeck and Wulff (2020) observe that clustering distance can be adversely affected by differences in cluster sizes. In our context, both $p_X(\psi_1, \psi_2)$ and $d_X(\psi_1, \psi_2)$ becomes problematic when h approaches n because there is then little room for the binary mappings ψ_1 and ψ_2 to disagree. For example, in the extreme situation $h = n$, both measures will be 0. For $p_X(\psi_1, \psi_2)$, to adjust for the effect of cluster sizes, we employ the scaled metric

$$p_X^c(\psi_1, \psi_2) = \frac{1}{c} p_X(\psi_1, \psi_2) \quad (9)$$

where $c = 2\frac{h}{n}\frac{(n-h)}{n}$ is the expectation of $|\psi_1(x_i) - \psi_2(x_i)|$ when ψ_1 and ψ_2 represent two randomly chosen inlier sets of size h from the rows of X . Sun et al. (2013) adopted a

similar scaling technique for tuning parameter selection in penalized regression. For a measure of instability based on the clustering distance, we follow [Haslbeck and Wulff \(2020\)](#) and employ the metric

$$d_X^c(\psi_1, \psi_2) = \frac{d_X(\psi_1, \psi_2)}{2c'(1-c')} - 1, \quad (10)$$

where $c' = \{\binom{h}{2} + \binom{n-h}{2}\} / \binom{n}{2}$ [Appendix A.5](#) gives the derivation of (10) and demonstrate that $c = 2\frac{h}{n}\frac{(n-h)}{n}$ is asymptotically equal to $1 - c'$ as n and h tend to infinity. Therefore, the two scaled distances are roughly comparable.

The average

$$\hat{s}(h, q) = \frac{1}{B} \sum_{b=1}^B d_X^c(\psi_{1,b}, \psi_{2,b}), \quad (11)$$

across B independent bootstrap pairs is our final measure of algorithmic instability. Here the binary maps $\psi_{1,b}$ and $\psi_{2,b}$ are subscripted by the bootstrap pair index b . If one is willing to average over correlated bootstrap samples, then $\hat{s}(h, q)$ can be replaced by

$$\hat{s}^*(h, q) = \frac{1}{\binom{B}{2}} \sum_{a < b} d_X^c(\psi_a, \psi_b) \quad (12)$$

using the pairwise dissimilarities between the $\binom{B}{2}$ pairs generated by B bootstrap samples.

[Algorithm 2](#) illustrates the workflow of our instability estimation algorithm using (10) as the dissimilarity measure and (11) as the instability measure. In practice, we search over a pre-set collection of pairs (h, q) to identify a parameter combination with minimal instability. Although [Algorithm 2](#) appears computationally intensive at first glance, many computational results can be recycled during a grid search. Specifically, we only need to compute the singular value decomposition and principal component projection once for each bootstrap sample. Given an identified h -subset, one can avoid Mahalanobis distances and use projection depth to distinguish outliers from inliers. For q fixed, the computed projection depths can be used for all values of h . We can also skip the concentration steps in [Algorithm 1](#) since a few outliers in the identified h -subset do not tangibly affect the binary mappings derived from projection depths.

[Figure 2](#) demonstrates the power of [Algorithm 2](#) in two examples, “Bull’s Eye” and “Exclamation Mark”, with 500 observations and 2 features each. “Bull’s Eye” has 200 points in the outer rim, while “Exclamation Mark” has 100 points in the bottom rectangle. We set $q = 2$ and apply [Algorithm 2](#) over the grid $h = 250, 275, \dots, 475$. As

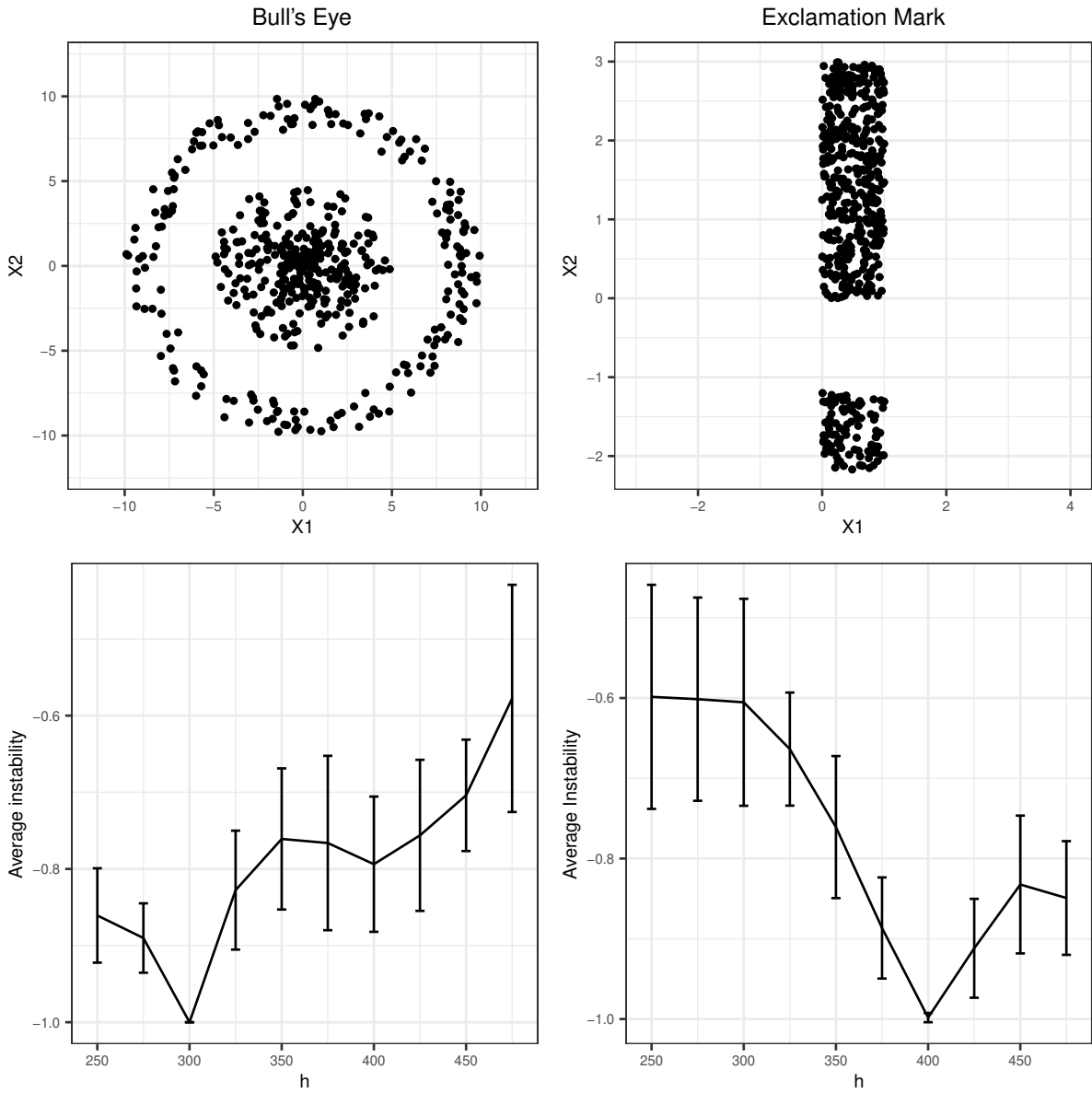


Figure 2: Top left panel is the generated example bull's eye. Bottom left panel is its instability path averaged over 50 bootstrap pairs, error bar denotes ± 1 standard deviation. Top right panel is the generated example exclamation mark. Bottom right panel is its instability path.

Algorithm 2 Instability Estimation

Input: Data matrix $X \in \mathbb{R}^{n \times p}$, subset size $h < n$, number of principal components $q \leq \min\{n, p\}$, number of random directions k , number of bootstrap pairs B .

- 1: **for** $b = 1 : B$ **do**
- 2: Construct a pair of bootstrapped samples \dot{X}_b and \ddot{X}_b .
- 3: Apply [Algorithm 1](#) to \dot{X}_b and \ddot{X}_b to obtain best h -subsets \dot{H}_b and \ddot{H}_b . As by-products, store the column means $\dot{\mu}_b$ and $\ddot{\mu}_b$ of \dot{X}_b and \ddot{X}_b , the right singular matrices \dot{V}_b and \ddot{V}_b , and the principal components \dot{Z}_b and \ddot{Z}_b .
- 4: Center and right multiply X by $(\dot{\mu}_b, \dot{V}_b[:, 1 : q])$ and $(\ddot{\mu}_b, \ddot{V}_b[:, 1 : q])$ respectively to obtain \dot{Z} and \ddot{Z} .
- 5: Compute projection depths $\dot{d}_i = D(\dot{z}_i; \dot{Z}_b[\dot{H}_b,])$, $\ddot{d}_i = D(\ddot{z}_i; \ddot{Z}_b[\ddot{H}_b,])$, $i = 1, 2, \dots, n$ with k random directions.
- 6: Set $\psi_{1,b}(x_i) = 0$ if \dot{d}_i is within the h -largest and $\psi_{1,b}(x_i) = 1$ otherwise. $\psi_{2,b}(x_i)$ is defined similarly.
- 7: Compute $d_X^c(\psi_{1,b}, \psi_{2,b})$ by equation (10).
- 8: **end for**

Output: $\hat{s}(h, q)$ in (11).

Figure 2 shows, [Algorithm 2](#) is able to correctly identify the number of observations in the dominant mode in both cases. We also examined how many observations the FDB algorithm ([Zhang et al., 2023](#)) designates as outliers. Here a point is categorized as an outlier if $w_i = 0$ in the reweighting step (6). Despite having a perfectly specified h , FDB estimates 62 outliers in the bull’s eye example and 64 outliers in the exclamation mark example, both of which are underestimations. This failure is likely due to the arbitrary cut-off value 0.975 in the reweighting step (6), which may not be universally suitable.

4 Simulation Studies

4.1 The Overdetermined Case $n > p$

In this section, we evaluate our method (SpectralMCD) under the simulation protocol used in the evaluation of both DetMCD ([Hubert et al., 2012](#)) and FDB ([Zhang et al., 2023](#)). The common protocol first generates inliers as $x_i = Gy_i$, where y_i is Gaussian $\mathcal{N}(0, I_p)$. The $p \times p$ matrix G has diagonal elements equal to 1 and off-diagonal elements equal to 0.75. The protocol then generates potential outliers at contamination levels of 10%, 25%, and 40%. The outliers are categorized into four types depending on a scalar r that determines the separation between inlier and outlier clusters.: (a) Point outliers $y_i \sim \mathcal{N}(ra\sqrt{p}, 0.01^2 I_p)$, where a is a unit vector orthogonal to $1 = (1, 1, \dots, 1)^\top$, (b) Cluster outliers $y_i \sim \mathcal{N}(rp^{-1/4}1, I_p)$, (c) Random outliers $y_i \sim \mathcal{N}(rp^{1/4}\nu_i/\|\nu_i\|, I_p)$, where

$\nu_i \sim \mathcal{N}(0, I_p)$, and (d) Radial outliers $y_i \sim \mathcal{N}(0, 5I_p)$. We use $r = 5$ throughout this section. Point, Cluster, and Radial outliers were introduced by [Hubert et al. \(2012\)](#) and Random outliers by [Zhang et al. \(2023\)](#).

We omit comparison with DetMCD since the experiments of [Zhang et al. \(2023\)](#) demonstrate that FDB performs almost uniformly better than DetMCD. For FDB, we assume no prior knowledge of the number of outliers and conservatively equate h to $\lfloor 0.5n \rfloor$, the breakdown point for MCD estimators. For SpectralMCD, we employ the following pipeline: (a) apply [Algorithm 2](#) to search over the grid $h = \lfloor 0.5n \rfloor, \lfloor 0.55n \rfloor, \dots, \lfloor 0.95n \rfloor$ and $q = 2, p$ to pinpoint the parameter combination (\hat{h}, \hat{q}) with the least average instability, (b) identify the optimal h -subset via [Algorithm 1](#) based on $(h, q) = (\hat{h}, \hat{q})$, and (c) estimate μ_X and Σ_X by the formulas [\(1\)](#). Unless stated to the contrary, we set the number of random directions $k = \max\{1000, 10q\}$. The outlier types Random and Radial seem to need a larger number of random directions for [Algorithm 2](#) to approximate projection depths accurately. Therefore, in these two scenarios we set $k = \max\{1000, 30q\}$. The estimators for the data set Y are then obtained as $\hat{\mu}_Y = G^{-1}\hat{\mu}_X$ and $\hat{\Sigma}_Y = G^{-1}\hat{\Sigma}_X G^{-1}$.

Our evaluation of the quality of these estimators relies on the following measures:

- $e_\mu = \|\hat{\mu}_Y - \mu_Y\|_2$, where μ_Y is the true mean vector of Y ; in this case $\mu_Y = 0$.
- $e_\Sigma = \log_{10}[\text{cond}(\hat{\Sigma}_Y \Sigma_Y^{-1})]$, where Σ_Y is the true covariance matrix of Y , and the operator cond finds the condition number of a matrix. In this case $\Sigma_Y = I_p$.
- The Kullback–Leibler divergence

$$\text{KL}(\hat{\Sigma}_Y, \Sigma_Y) = \text{tr}(\hat{\Sigma}_Y \Sigma_Y^{-1}) - \log\{\det(\hat{\Sigma}_Y \Sigma_Y^{-1})\} - p \quad (13)$$

depending on the matrix trace operator.

We consider three combinations of n and p : $(n, p) = (400, 40)$, $(n, p) = (400, 80)$, and $(n, p) = (2000, 200)$. [Table 1](#) and [Table 2](#) list results for the combination $(n, p) = (400, 40)$ and $(n, p) = (400, 80)$; the results for $(n, p) = (2000, 200)$ and statistics on computation time appear in [Appendix B](#).

[Table 1](#) and [Table 2](#) show that our pipeline consistently offers more precise estimates than FDB, particularly in estimating Σ . Because SpectralMCD tries to incorporate as many observations as possible, its advantage becomes more pronounced as the proportion of outliers decreases. As p goes from 40 to 80, the performance of FDB deteriorates, and

Table 1: Simulation results when $(n, p) = (400, 40)$. All measures are averaged over 50 random replicates. The numbers in parentheses are standard errors. Abbreviations are KL: Kullback–Leibler divergence, FDB: fast depth-based method algorithm, and Spec: spectral minimum covariance determinant.

Outlier	Metric	10%		25%		40%	
		FDB	Spec	FDB	Spec	FDB	Spec
Point	e_μ	0.346	0.320	0.379	0.366	25.30	1.358
		(0.035)	(0.030)	(0.044)	(0.045)	(0.100)	(3.881)
	e_Σ	0.629	0.567	0.659	0.623	6.113	0.903
		(0.031)	(0.023)	(0.032)	(0.027)	(0.244)	(0.693)
	KL	2.870	2.375	3.148	2.826	231.1	18.54
		(0.163)	(0.096)	(0.191)	(0.153)	(2.744)	(58.79)
Cluster	e_μ	0.351	0.328	0.369	0.355	0.405	0.400
		(0.037)	(0.034)	(0.035)	(0.037)	(0.040)	(0.038)
	e_Σ	0.624	0.566	0.658	0.619	0.722	0.712
		(0.032)	(0.026)	(0.036)	(0.025)	(0.029)	(0.027)
	KL	2.843	2.383	3.180	2.864	3.753	3.631
		(0.177)	(0.107)	(0.187)	(0.137)	(0.189)	(0.193)
Random	e_μ	0.358	0.336	0.380	0.366	0.407	0.400
		(0.039)	(0.035)	(0.043)	(0.043)	(0.050)	(0.051)
	e_Σ	0.624	0.558	0.658	0.621	0.711	0.698
		(0.027)	(0.024)	(0.026)	(0.024)	(0.028)	(0.025)
	KL	2.853	2.358	3.177	2.878	3.732	3.597
		(0.169)	(0.108)	(0.155)	(0.134)	(0.175)	(0.155)
Radial	e_μ	0.354	0.328	0.369	0.355	0.407	0.401
		(0.039)	(0.034)	(0.039)	(0.037)	(0.040)	(0.038)
	e_Σ	0.624	0.566	0.656	0.619	0.723	0.711
		(0.032)	(0.026)	(0.030)	(0.025)	(0.026)	(0.027)
	KL	2.837	2.383	3.184	2.864	3.748	3.632
		(0.174)	(0.107)	(0.187)	(0.137)	(0.189)	(0.193)

Table 2: Simulation results for $(n, p) = (400, 80)$. All measures are averaged over 50 random replicates. The numbers in parentheses are standard errors. Abbreviations are KL: Kullback–Leibler divergence, FDB: fast depth-based algorithm, and Spec: spectral minimum covariance determinant.

Outlier	Metric	10%		25%		40%	
		FDB	Spec	FDB	Spec	FDB	Spec
Point	e_μ	0.575	0.469	0.605	0.522	35.52	3.057
		(0.049)	(0.037)	(0.048)	(0.045)	(1.320)	(7.715)
	e_Σ	1.125	0.855	1.161	0.956	7.122	1.555
		(0.039)	(0.027)	(0.038)	(0.028)	(0.334)	(1.424)
	KL	15.98	9.771	16.79	11.91	679.9	68.03
		(0.784)	(0.262)	(0.727)	(0.254)	(23.96)	(158.7)
Cluster	e_μ	0.579	0.465	0.610	0.518	0.621	0.585
		(0.053)	(0.039)	(0.052)	(0.043)	(0.053)	(0.045)
	e_Σ	1.138	0.856	1.165	0.958	1.201	1.100
		(0.043)	(0.022)	(0.039)	(0.025)	(0.038)	(0.034)
	KL	16.22	9.776	16.75	11.97	17.70	15.39
		(0.760)	(0.248)	(0.716)	(0.304)	(0.574)	(0.389)
Random	e_μ	0.582	0.467	0.601	0.519	0.607	0.572
		(0.053)	(0.037)	(0.051)	(0.036)	(0.052)	(0.052)
	e_Σ	1.143	0.862	1.173	0.952	1.215	1.109
		(0.037)	(0.022)	(0.044)	(0.028)	(0.038)	(0.038)
	KL	16.11	9.770	16.92	11.94	18.02	15.58
		(0.619)	(0.213)	(0.658)	(0.302)	(0.593)	(0.680)
Radial	e_μ	0.586	0.465	0.594	0.518	0.627	0.585
		(0.054)	(0.039)	(0.054)	(0.043)	(0.050)	(0.045)
	e_Σ	1.143	0.856	1.167	0.958	1.215	1.110
		(0.043)	(0.022)	(0.05)	(0.025)	(0.043)	(0.034)
	KL	16.42	9.776	16.82	11.97	18.07	15.39
		(0.852)	(0.248)	(0.852)	(0.304)	(0.579)	(0.389)

the comparative advantage of SpectralMCD becomes more evident. The deterioration of FDB might be due to the fact that the reweighting step (6) becomes less reliable as p grows. Additionally, it is evident that Algorithm 2 effectively selected the appropriate h across nearly all scenarios, except for the Point outliers scenario at a 40% outlier level. In this particular setting, both methods struggle to identify numerous outliers, and estimation is fraught with significant errors. We speculate that this specific setting is statistically impossible for MCD estimators. The Random scenario with outlier proportion 40% is the only other scenario where Algorithm 2 does not perfectly select the true number of inliers. In this case Algorithm 2 selects $h = \lfloor 0.55n \rfloor$ half of the time. Finally, it is worth noting that while our pipeline yields more accurate estimates, it does so at the expense of a computationally intensive bootstrap procedure that takes considerably longer to run than the two baseline methods. Consult Table 4 in Appendix B for specific timing comparisons.

4.2 The Underdetermined Case $p > n$

In this section, we compare our method (SpectralMCD) to minimum regularized covariance determinant (MRCD) (Boudt et al., 2020) and FDB (Zhang et al., 2023) in the underdetermined case $p > n$. In this setting the sample covariance matrix is singular, and FDB’s reweighting step must be skipped. We adopt the simulation protocol of Boudt et al. (2020), but extend p beyond the range previously considered. Without loss of generality, we set the mean vector $\mu \in \mathbb{R}^p$ to 0. The covariance matrix Σ is constructed iteratively to ensure that its condition number (CN) closely approximates 50. Section 4 of (Agostinelli et al., 2015) explains in detail this covariance matrix generation protocol. Our simulated outliers are generated from the distribution $\mathcal{N}(50a, \Sigma)$, where a is the unit eigenvector corresponding to the smallest eigenvalue of Σ . This setup is intentionally crafted so that the direction a poses the greatest difficulty in outlier detection.

As in Section 4.1, we put $h = \lfloor 0.5n \rfloor$ for the two baseline methods. We first apply Algorithm 2 to search over the grid $h = \lfloor 0.5n \rfloor, \lfloor 0.55n \rfloor, \dots, \lfloor 0.95n \rfloor$ and $q = 2, 10, 100$. To its credit, Algorithm 2 consistently selects the correct h and $q = 2$ for each replicate across all values of p . Subsequently, we apply Algorithm 1 to identify the outliers at the optimal parameter combination. For all three methods, once the h -subset is obtained, we

follow [Boudt et al. \(2020\)](#) in computing the final estimate

$$\hat{\Sigma}_\rho = \rho I + (1 - \rho)\hat{\Sigma}_H \quad (14)$$

of Σ , where $\hat{\Sigma}_H$ is the sample covariance matrix based on the subset H . The parameter ρ is determined so that $\hat{\Sigma}_\rho$ has the desired condition number CN . Forcing the generated positive definite covariance matrices to have a common condition number places the three methods SpectralMCD, MRCD, and FDB on an equal footing for comparison. We evaluate the statistical precision of the three methods using the metrics e_μ and Kull-

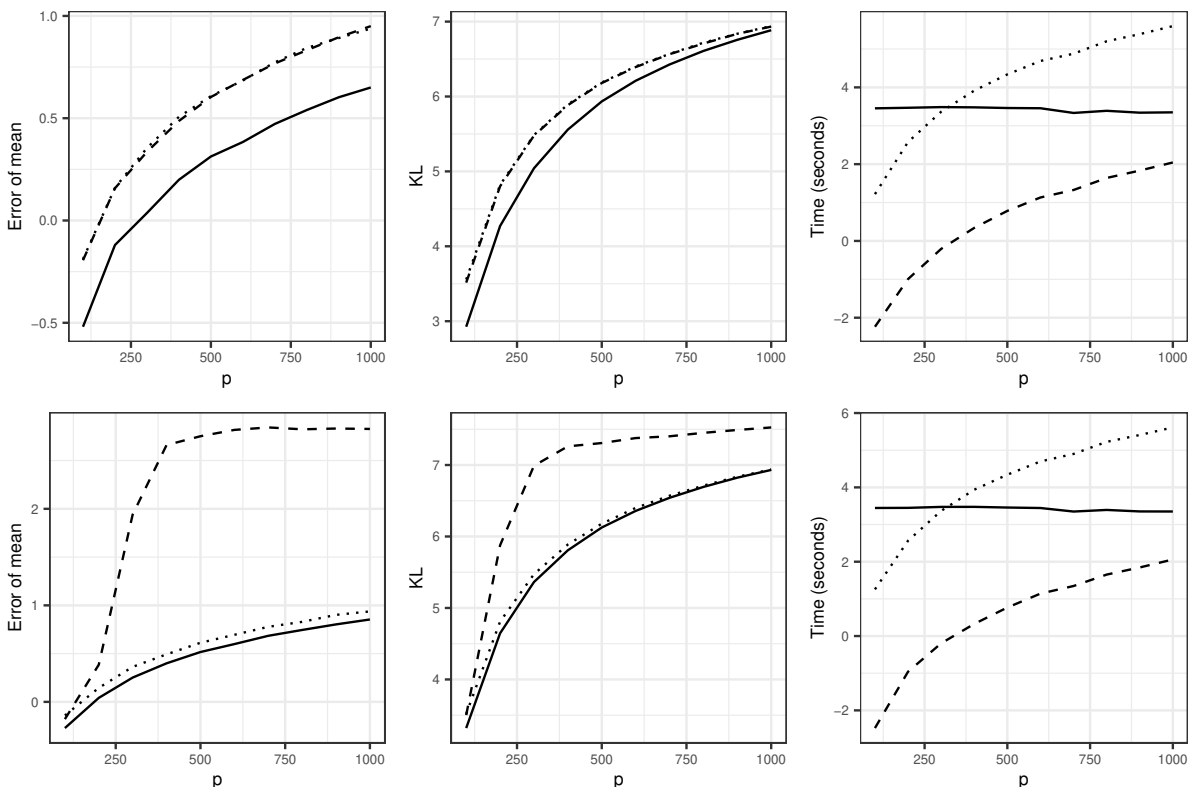


Figure 3: Experimental results for high-dimensional data. First and second row corresponds to outlier level 10% and 40%, respectively. Data points are averaged over 20 replicates. The y-axis for all panels are transformed to log scale for better visualization. Solid line stands for SpectralMCD, dashed line for FDB, and dotted line for MRCD.

back–Leibler divergence defined in [Section 4.1](#). Additionally, we measure total elapsed time to assess computational efficiency. For our method, the total elapsed time includes the time required for the grid search to identify the optimal parameter combination. Fixing n at 300, we vary p over the range 100, 200, \dots , 1000.

[Figure 3](#) depicts the experimental results. By incorporating more observations, our pipeline consistently offers better statistical precision than the two baseline methods. The

computation time of MRCD appears to scale cubically with p , while the computation time of our workflow (including grid search) remains almost constant. As a result, when p grows sufficiently large, our workflow becomes more efficient than MRCD, even though we invoke a costly bootstrap procedure to search for the best parameter combination. In general, FDB is lightning quick compared to the other two methods. However, when the outlier proportion reaches 40%, it unfortunately breaks down and yields large estimation errors. Although our workflow is also based on projection depth, it remains robust even with this simplification. This again highlights the virtue of using the principal component transform to reveal the hidden low-dimensional structure of the data.

5 Real Data Examples

5.1 Fruit Data

Our first real data example, referred to as the fruit data, comprises spectra from three distinct cantaloupe cultivars, labeled D, M, and HA with sample sizes of 490, 106, and 500, respectively. Originally introduced by [Hubert and Van Driessen \(2004\)](#) and later examined by [Hubert et al. \(2012\)](#), these data encompass 1096 total observations recorded across 256 wavelengths. [Hubert and Van Driessen \(2004\)](#) note that the cultivar HA encompasses three distinct groups derived from various illumination systems. Unfortunately, the assignment of individual observations to specific subgroups and the potential impact of the subgroups on spectra is unavailable.

Our purpose is to estimate the number of outliers and decide which observations qualify as outliers. FDB with $h = \lfloor 0.5n \rfloor$ is our the baseline method. As in [Section 3.3](#), an observation x_i is flagged by FDB as an outlier when w_i in the reweighting step [\(6\)](#) equals 0. For our method, we applied [Algorithm 2](#) over the grid $h = \lfloor 0.5n \rfloor, \lfloor 0.55n \rfloor, \dots, \lfloor 0.95n \rfloor$ with $q = 2$ principal components. The grid search over 50 bootstrap pairs took 57 seconds to complete. We then applied [Algorithm 1](#) to identify the inliers and outliers using the optimal parameter combination. The choice of $q = 2$ is motivated by a scree plot demonstrating that nearly all variance can be explained using just two principal components ([Hubert et al., 2012](#)).

[Figure 4](#) depicts the experimental outcomes. The left panel of [Figure 4](#) shows the first two principal components of the data set, with each point colored by the corresponding cultivar. Evidently, observations significantly diverging from the primary mode almost

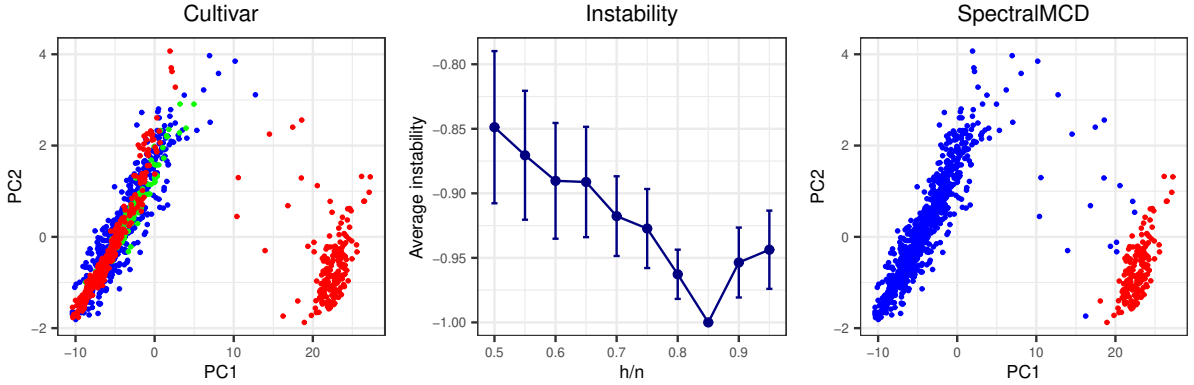


Figure 4: Experimental results for the fruit data set. In the left panel, cultivar D points are colored blue, cultivar M points are colored green, and cultivar HA points are colored red. In the right panel, blue points are inliers while red points are outliers.

exclusively belong to the HA cultivar. The middle panel displays the instability path computed by [Algorithm 2](#), which is minimized at $h = \lfloor 0.85n \rfloor$. The right panels illustrate the assignment of inliers and outliers identified by SpectralMCD based on the parameter combination $(h = \lfloor 0.85n \rfloor, q = 2)$. SpectralMCD appears quite effective in segregating the two modes, although there are a few points far away from the primary mode that are not assigned as outliers. This might be due to the fact that our search grid is not fine grained enough. FDB in this example categorizes 497 points as outliers using a cut-off of 0.975, which is hard to interpret given the principal component visualization. We suspect that the reweighting procedure [\(6\)](#) might have failed due to the ill conditioning of the estimated covariance matrix. [Algorithm 2](#) estimates approximately $1096 \times 0.15 \approx 164$ outliers, roughly a third of the 500 observations. We conjecture that the outliers in the HA cultivar correspond to a subgroup with a distinctive illumination pattern.

5.2 Breast Cancer Data

Our second real data example comes from the The Cancer Genome Atlas (TCGA) project ([Network, 2012](#)). The breast cancer project (TCGA-BRCA) contains data on approximately 1100 patients with invasive carcinoma of the breast. Our data is sourced from cBioPortal¹ ([Cerami et al., 2012](#)). We focus on the mRNA expression profiles of the patients. These profiles represent expression levels for 20531 genes on the 1100 samples. After performing a $\log_2(x + 1)$ transform on the expression levels, we retained the top 2000 most variable genes. Apart from expression profiles, the data also record the estro-

¹<https://www.cbioportal.org/>

gen receptor (ER) status of each sample. Women with estrogen receptor negative status (ER-) are typically diagnosed at a younger age and have a higher mortality rate (Bauer et al., 2007). Out of 1100 samples, 812 are estrogen receptor positive, 238 are negative, 48 are indeterminate, and 2 are missing. We retain the 1050 samples for which the estrogen receptor status is either positive or negative. Thus, our preprocessed data matrix has dimension 1050×2000 .

As in Section 5.1, we first applied Algorithm 2 to estimate the proportion of outliers in the data set. Unlike the fruit data set, a scree plot for these data reveals a wider spread of the variance across many principal components. Therefore, we searched via Algorithm 2 over a two-dimensional parameter grid $q = 2, 10, 100$ and $h = \lfloor 0.5n \rfloor, \lfloor 0.55n \rfloor, \dots, \lfloor 0.95n \rfloor$. The grid search takes 968 seconds to complete. We then applied Algorithm 1 to identify the outliers under this optimal parameter combination. Figure 5 depicts the experimen-

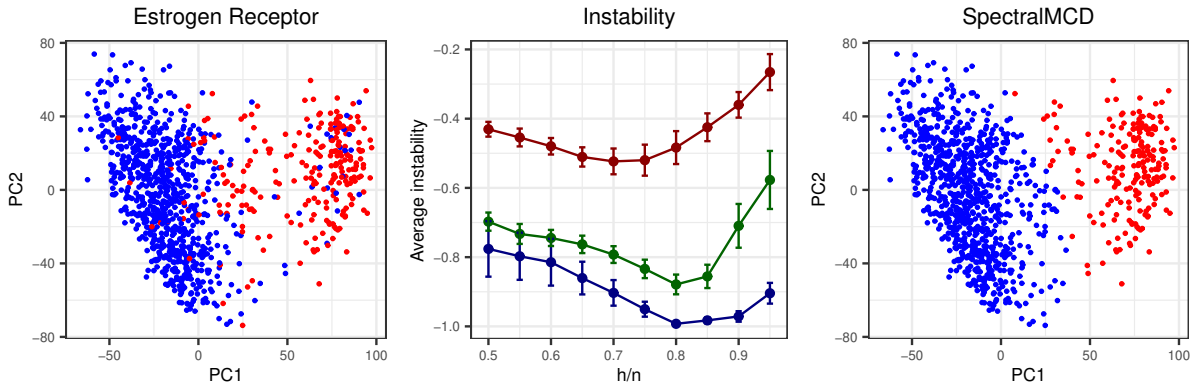


Figure 5: Experimental results for the breast cancer data set. In the left panel, blue points are estrogen receptor positive, red points are negative. In the middle panel, blue, green, red lines are instability paths at $q = 2$, $q = 10$, $q = 100$. In the right panel, blue points are inliers while red points are outliers.

tal results. At $q = 2$ and 10 , the instability is minimized at $h = \lfloor 0.8n \rfloor$. However, at $q = 100$, the instability is minimized at $h = \lfloor 0.7n \rfloor$. Possibly the redundant principal components obscure the inlier/outlier structure. To minimize algorithmic instability, we select the optimal parameter combination $(h, q) = (\lfloor 0.8n \rfloor, 2)$. In the general population, about 79-84% of breast cancer cases will be estrogen receptor positive (Allison et al., 2020). Our algorithms are able to infer this medical fact purely from the gene expression profile without reference to recorded estrogen receptor status. Moreover, if we consider this problem as a binary classification problem, Algorithm 1 achieves an unsupervised classification accuracy of 92.4%.

6 Discussion

This paper introduces several improvements to the minimum covariance determinant (MCD) procedure. We use principal components to uncover the hidden low-dimensional structure of inlier/outlier distribution which enhances outlier detection efficacy. Projection depths emerge as effective initiators for the MCD search process. Additionally, our bootstrap methodology enables us to identify the appropriate subset size and number of principal components (q), thereby proving invaluable in robust estimation and outlier detection. Our appendix relates MCD to maximum likelihood estimation, clarifies univariate MCD, and suggests some algorithmic improvements to traditional MCD.

Our SpectralMCD method is rigorously evaluated against well-established variants of the minimum covariance determinant (MCD) algorithm, namely the fast depth-based algorithm (FDB) and minimum regularized covariance determinant (MRCD). In direct comparison, SpectralMCD excels in accurately estimating the number of outliers and advocates for leveraging a larger portion of observations in estimating location and scatter parameters. Notably, in high-dimensional scenarios, SpectralMCD circumvents the computational burden of matrix inversions, showcasing superior computational efficiency compared to regularized MCD. These findings are substantiated by our comprehensive analysis on both simulated and real-world datasets.

Acknowledgement

We thank Seyoon Ko and Do Hyun Kim for useful suggestions. This research was partially funded by USPHS grants GM53275 and HG006139.

A Proofs and Algorithm Improvements

A.1 Proof of Proposition 2.1 and Corollary 2.1

Proof. It is well known that the maximum likelihood estimates of μ and Σ are

$$\bar{x} = \frac{1}{h} \sum_{i=1}^n w_i x_i \quad \text{and} \quad \hat{\Sigma} = \frac{1}{h} \sum_{i=1}^n w_i (x_i - \bar{x})(x_i - \bar{x})^\top.$$

For instance, see Example 11.2.3 of (Lange, 2010). Given these estimates, the loss (4) becomes

$$\begin{aligned} & h \log(\det \hat{\Sigma}) + \sum_{i=1}^n w_i (x_i - \bar{x})^\top \hat{\Sigma}^{-1} (x_i - \bar{x}) \\ &= h \log(\det \hat{\Sigma}) + \text{tr} \left[\hat{\Sigma}^{-1} \sum_{i=1}^n w_i (x_i - \bar{x})(x_i - \bar{x})^\top \right] \\ &= h \log(\det \hat{\Sigma}) + \text{tr}(\hat{\Sigma}^{-1} \hat{\Sigma}) \\ &= h \log(\det \hat{\Sigma}) + hp. \end{aligned}$$

Thus, minimizing the loss (4) is equivalent to minimizing $\det \hat{\Sigma}$.

To prove Corollary 2.1, we write the objective in (4) as $f(\mu, \Sigma, w)$. Given the current iterate $(\mu^{(t)}, \Sigma^{(t)}, w^{(t)})$, the next iterate minimizes $f(\mu, \Sigma, w^{(t)})$ with respect to μ and Σ via equation (1) and then minimizes $f(\mu^{(t+1)}, \Sigma^{(t+1)}, w)$ with respect to w via Equation (3). This produces

$$f(\mu^{(t+1)}, \Sigma^{(t+1)}, w^{(t+1)}) \leq f(\mu^{(t+1)}, \Sigma^{(t+1)}, w^{(t)}) \leq f(\mu^{(t)}, \Sigma^{(t)}, w^{(t)})$$

so that

$$f(\mu^{(t+1)}, \Sigma^{(t+1)}, w^{(t+1)}) = h \log(\det \hat{\Sigma}^{(t+1)}) + hp \leq h \log(\det \hat{\Sigma}^{(t)}) + hp = f(\mu^{(t)}, \Sigma^{(t)}, w^{(t)}),$$

which implies $\det \hat{\Sigma}^{(t+1)} \leq \det \hat{\Sigma}^{(t)}$. □

A.2 Proof of Proposition 3.1

Proof. Because $q = p$, the right singular matrix V is a $p \times p$ orthogonal matrix. Centering does not change the sample covariance matrix, so $\hat{\Sigma}(X_H) = \hat{\Sigma}(\tilde{X}_H)$. Given that the right

singular matrix V is invertible,

$$\det[\hat{\Sigma}(Z_H)] = \det[\hat{\Sigma}(\tilde{X}_H V)] = \det[V^\top \hat{\Sigma}(\tilde{X}_H) V] = \det(V)^2 \det[\hat{\Sigma}(\tilde{X}_H)].$$

Thus, any h -subset H that minimizes $\det[\hat{\Sigma}(Z_H)]$ also minimizes $\det[\hat{\Sigma}(X_H)]$ and vice-versa.

The location invariance of SpectralMCD follows from the fact that we center the data matrix as a first step. To prove permutation invariance, assume that the centered matrix \tilde{X} has thin SVD $\tilde{X} = USV^\top$. Now consider a permutation matrix $P \in \mathbb{R}^{n \times n}$. Since any permutation matrix is orthogonal, $P\tilde{X} = (PU)SV^\top$, and (PU, S, V) is the SVD tuple of the permuted matrix $P\tilde{X}$. The new principal component score matrix is then $Z_P = (PU)SV^\top V[:, 1 : q] = PU[:, 1 : q]S[1 : q, 1 : q] = PZ$, where Z is the original principal component score matrix. Permutation invariance now follows from the fact that the original MCD problem is permutation invariant. \square

A.3 Proof of Proposition 3.2

Proof. The spectral MCD problem is the MCD problem defined on the principal component matrix Z . If μ_z and Σ_z are the maximum likelihood estimates of μ and Σ given the previous H , then

$$\begin{aligned} (z_i - \mu_z)^\top \Sigma_z^{-1} (z_i - \mu_z) &\leq r, \quad \forall i \in H \\ (z_i - \mu_z)^\top \Sigma_z^{-1} (z_i - \mu_z) &\geq r, \quad \forall i \in H^c \end{aligned}$$

for the current H and some r . For notational simplicity, write $V[:, 1 : q]$ as \tilde{V} and the column mean vector of X as \bar{x} . The vectors z_i are obtained through $z_i = \tilde{V}^\top (x_i - \bar{x})$. Hence,

$$\begin{aligned} (\tilde{V}^\top (x_i - \bar{x}) - \mu_z)^\top \Sigma_z^{-1} (\tilde{V}^\top (x_i - \bar{x}) - \mu_z) &\leq r, \quad \forall i \in H \\ (\tilde{V}^\top (x_i - \bar{x}) - \mu_z)^\top \Sigma_z^{-1} (\tilde{V}^\top (x_i - \bar{x}) - \mu_z) &\geq r, \quad \forall i \in H^c, \end{aligned}$$

which implies that H is separated from H^c by the quadratic function

$$f(x) = x^\top \tilde{V} \Sigma_z^{-1} \tilde{V}^\top x - 2(\tilde{V}^\top \bar{x} + \mu_z)^\top \Sigma_z^{-1} \tilde{V}^\top x + (\tilde{V}^\top \bar{x} + \mu_z)^\top \Sigma_z^{-1} (\tilde{V}^\top \bar{x} + \mu_z) - r.$$

After a finite numbers of iterations, H , μ , and Σ stabilize. Conceivably, the algorithm can cycle between equally favorable subsets, so it should be stopped when no further gains are realized. \square

A.4 Proof of Proposition 3.3

Proof. Let A and B denote the h-subsets selected by ψ_1 and ψ_2 from $\{x_1, x_2, \dots, x_n\}$. Suppose $A\Delta B$ denotes the symmetric difference of the sets A and B . The binary map distance can be expressed as an expectation involving two independent random variables X and Y uniformly distributed over the set $\{1, 2, \dots, n\}$. In this context the distance between A and B amounts to

$$\begin{aligned}
p_X(\psi_1, \psi_2) &= E[|I_A(X)I_A(Y) + I_{A^c}(X)I_{A^c}(Y) - I_B(X)I_B(Y) - I_{B^c}(X)I_{B^c}(Y)|] \\
&= E\{[I_A(X)I_A(Y) + I_{A^c}(X)I_{A^c}(Y) - I_B(X)I_B(Y) - I_{B^c}(X)I_{B^c}(Y)]^2\} \\
&= \Pr(A)^2 + \Pr(A^c)^2 + \Pr(B)^2 + \Pr(B^c)^2 - 2\Pr(A \cap B)^2 \\
&\quad - 2\Pr(A \cap B^c)^2 - 2\Pr(A^c \cap B)^2 - 2\Pr(A^c \cap B^c)^2 \\
&= [\Pr(A \cap B) + \Pr(A \cap B^c)]^2 + [\Pr(A^c \cap B) + \Pr(A^c \cap B^c)]^2 \\
&\quad + [\Pr(A \cap B) + \Pr(A^c \cap B)]^2 + [\Pr(A \cap B^c) + \Pr(A^c \cap B^c)]^2 \\
&\quad - 2\Pr(A \cap B)^2 - 2\Pr(A \cap B^c)^2 - 2\Pr(A^c \cap B)^2 - 2\Pr(A^c \cap B^c)^2 \\
&= 2\Pr(A \cap B)\Pr(A \cap B^c) + 2\Pr(A^c \cap B)\Pr(A^c \cap B^c) \\
&\quad + 2\Pr(A \cap B)\Pr(A^c \cap B) + 2\Pr(A \cap B^c)\Pr(A^c \cap B^c) \\
&= 2[\Pr(A \cap B) + \Pr(A^c \cap B^c)]\Pr(A\Delta B) \\
&= 2[1 - \Pr(A\Delta B)]\Pr(A\Delta B).
\end{aligned}$$

We also provide a direct proof with algebra. We have

$$\begin{aligned}
p_X(\psi_1, \psi_2)[1 - p_X(\psi_1, \psi_2)] &= \frac{1}{n} \sum_{i=1}^n |\psi_1(x_i) - \psi_2(x_i)| \left[1 - \frac{1}{n} \sum_{i=1}^n |\psi_1(x_i) - \psi_2(x_i)| \right] \\
&= \frac{1}{n^2} \sum_{i=1}^n |\psi_1(x_i) - \psi_2(x_i)| \sum_{i=1}^n [1 - |\psi_1(x_i) - \psi_2(x_i)|] \\
&= \frac{1}{n^2} \sum_{i=1}^n \sum_{j=1}^n |\psi_1(x_i) - \psi_2(x_i)| [1 - |\psi_1(x_j) - \psi_2(x_j)|]
\end{aligned}$$

Because

$$|\psi_1(x_i) - \psi_2(x_i)| = I_{\psi_1(x_i) \neq \psi_2(x_i)} \quad \text{and} \quad 1 - |\psi_1(x_j) - \psi_2(x_j)| = I_{\psi_1(x_j) = \psi_2(x_j)},$$

$$p_X(\psi_1, \psi_2)[1 - p_X(\psi_1, \psi_2)] = \frac{1}{n^2} \sum_{i=1}^n \sum_{j=1}^n I_{\psi_1(x_i) \neq \psi_2(x_i)} I_{\psi_1(x_j) = \psi_2(x_j)}.$$

By symmetry of (i, j) , we can also write

$$p_X(\psi_1, \psi_2)[1 - p_X(\psi_1, \psi_2)] = \frac{1}{n^2} \sum_{i=1}^n \sum_{j=1}^n I_{\psi_1(x_j) \neq \psi_2(x_j)} I_{\psi_1(x_i) = \psi_2(x_i)}.$$

Therefore

$$\begin{aligned} & 2p_X(\psi_1, \psi_2)[1 - p_X(\psi_1, \psi_2)] \\ &= \frac{1}{n^2} \sum_{i=1}^n \sum_{j=1}^n [I_{\psi_1(x_i) \neq \psi_2(x_i)} I_{\psi_1(x_j) = \psi_2(x_j)} + I_{\psi_1(x_j) \neq \psi_2(x_j)} I_{\psi_1(x_i) = \psi_2(x_i)}], \end{aligned}$$

and simple enumeration of all 16 possible choices of $\psi_1(x_i)$, $\psi_2(x_i)$, $\psi_1(x_j)$, and $\psi_2(x_j)$ implies

$$I_{\psi_1(x_i) \neq \psi_2(x_i)} I_{\psi_1(x_j) = \psi_2(x_j)} + I_{\psi_1(x_j) \neq \psi_2(x_j)} I_{\psi_1(x_i) = \psi_2(x_i)} = |I_{\psi_1(x_i) = \psi_1(x_j)} - I_{\psi_2(x_i) = \psi_2(x_j)}|.$$

Thus, we have

$$d_X(\psi_1, \psi_2) = 2p_X(\psi_1, \psi_2)[1 - p_X(\psi_1, \psi_2)].$$

□

A.5 Derivation of the Corrected Clustering Distance

We follow the arguments in [Haslbeck and Wulff \(2020\)](#). Under the simplifying assumption that $\psi_1(x_i) = \psi_1(x_j)$ and $\psi_2(x_i) = \psi_2(x_j)$ are equally likely for all pairs of (i, j) , symmetry entails

$$\begin{aligned} \mathbb{E}[d_X(\psi_1, \psi_2)] &= \mathbb{E}[|I_{\psi_1(x_i) = \psi_1(x_j)} - I_{\psi_2(x_i) = \psi_2(x_j)}|] \\ &= \mathbb{E}[I_{\psi_1(x_i) = \psi_1(x_j)} I_{\psi_2(x_i) \neq \psi_2(x_j)} + I_{\psi_1(x_i) \neq \psi_1(x_j)} I_{\psi_2(x_i) = \psi_2(x_j)}] \\ &= 2\mathbb{E}\{I_{\psi_1(x_i) = \psi_1(x_j)} [1 - I_{\psi_2(x_i) = \psi_2(x_j)}]\}, \end{aligned}$$

where the third equality is due to the symmetry of ψ_1 and ψ_2 . In view of the covariance identity $E(XY) = E(X)E(Y) + \text{Cov}(X, Y)$, we have

$$\begin{aligned} E\{\mathbf{I}_{\psi_1(x_i)=\psi_1(x_j)}[1 - \mathbf{I}_{\psi_2(x_i)=\psi_2(x_j)}]\} &= E[\mathbf{I}_{\psi_1(x_i)=\psi_1(x_j)}]E[1 - \mathbf{I}_{\psi_2(x_i)=\psi_2(x_j)}] \\ &+ \text{Corr}[\mathbf{I}_{\psi_1(x_i)=\psi_1(x_j)}, 1 - \mathbf{I}_{\psi_2(x_i)=\psi_2(x_j)}] \sqrt{\text{Var}[\mathbf{I}_{\psi_1(x_i)=\psi_1(x_j)}]} \sqrt{\text{Var}[1 - \mathbf{I}_{\psi_2(x_i)=\psi_2(x_j)}]}. \end{aligned}$$

Our Bernoulli event assumption implies that

$$\begin{aligned} E[\mathbf{I}_{\psi_1(x_i)=\psi_1(x_j)}] &= E[\mathbf{I}_{\psi_2(x_i)=\psi_2(x_j)}] = c' = \left[\binom{h}{2} + \binom{n-h}{2} \right] / \binom{n}{2}, \\ \text{Var}[\mathbf{I}_{\psi_1(x_i)=\psi_1(x_j)}] &= \text{Var}[1 - \mathbf{I}_{\psi_2(x_i)=\psi_2(x_j)}] = c'(1 - c'). \end{aligned}$$

Thus, in estimating $\text{Corr}[\mathbf{I}_{\psi_1(x_i)=\psi_1(x_j)}, 1 - \mathbf{I}_{\psi_2(x_i)=\psi_2(x_j)}]$, it is reasonable to employ the metric

$$d_X^c(\psi_1, \psi_2) = \frac{d_X(\psi_1, \psi_2)}{2c'(1 - c')} - 1.$$

Observe that

$$1 - c' = 1 - \left[\binom{h}{2} + \binom{n-h}{2} \right] / \binom{n}{2} = 1 - \frac{h(h-1) + (n-h)(n-h-1)}{n(n-1)},$$

and recall the definition of

$$c = \frac{2h(n-h)}{n^2} = 1 - \frac{h^2 + (n-h)^2}{n^2}$$

from equation (12). Since $h^2 \asymp h(h-1)$, $n^2 \asymp n(n-1)$, $n^2 \asymp n(n-1)$, c and $1 - c'$ are asymptotically equivalent and negligibly different when n and h are large.

A.6 Exact Solution for Univariate MCD

Hubert and Debruyne (2010) mention that the univariate minimum covariance determinant problem can be solved in $O(n \log n)$ operations by operating on successive windows of h -subsets. Surprisingly, we can not find a detailed justification of this claim in the literature. We now describe in detail the univariate algorithm and prove that it indeed solves the minimum variance problem. In the univariate case, minimum covariance determinant reduces to finding $h < n$ observations among x_1, x_2, \dots, x_n with minimal sample variance. The solution procedure involves sorting x_1, x_2, \dots, x_n and then sliding a window

of length h along the the sorted array. At each position of the window, the sample mean and sample variance are updated, and the sample variance is recorded. A best subset minimizes the $n - h$ recorded sample variances. Specifically, if the order statistics are denoted by $y_1 \leq y_2 \leq \dots \leq y_n$, then the first window consists of observations y_1, y_2, \dots, y_h , with sample mean and variance

$$\mu_h = \frac{1}{h} \sum_{i=1}^h y_i \quad \text{and} \quad \sigma_h^2 = \frac{1}{h} \sum_{i=1}^h (y_i - \mu_h)^2.$$

As we move the window to the right one position, the Welford's formulas ([Welford, 1962](#)) update these two statistics via

$$\begin{aligned} \mu_{h+1} &= \frac{1}{h+1} (h\mu_h + y_{h+1}), \\ \sigma_{h+1}^2 &= \frac{h}{h+1} \sigma_h^2 + \frac{1}{h} (y_{h+1} - \mu_{h+1})^2, \\ \mu_h &= \frac{1}{h} [(h+1)\mu_{h+1} - y_1], \\ \sigma_h^2 &= \frac{h+1}{h} \sigma_{h+1}^2 - \frac{h+1}{h^2} (y_1 - \mu_{h+1})^2 \end{aligned}$$

at a cost of $O(1)$. The updated sample variance is added to the growing list of sample variances. We repeat this process until the reaching the last window with right endpoint y_n . Tracking the minimal σ_h^2 encountered as well as its corresponding starting and ending positions solves the problem at a cost of $O(n \log n)$, which is dominated by sorting.

To convince readers that this algorithm finds the optimal h -subset, we argue by contradiction. Consider a subset S that possesses the lowest subset variance. Within S , let l and u represent the smallest and largest numbers, respectively. Now suppose we select any number x from the entire sample such that $l < x < u$, but x is not included in the subset S . Let us substitute x for l if $x \leq \bar{x}_S$ and for u if $x > \bar{x}_S$. This results in a new subset, which we denote as T . We clearly have

$$\sum_{i \in T} (x_i - \bar{x}_T)^2 \leq \sum_{i \in T} (x_i - \bar{x}_S)^2 < \sum_{i \in S} (x_i - \bar{x}_S)^2,$$

which contradicts the assumption that S is the subset with the lowest variance. Thus, any observation that falls between (l, u) must also fall in the subset. In other words, the optimal subset must occupy a contiguous window among the order statistics.

A.7 Efficient Implementation of FastMCD

The main computational bottlenecks of the fast minimum covariance determinant algorithm are the concentration steps. These require repeated evaluation of the matrix inverse Σ^{-1} and determinant $\det \Sigma$. Here we describe a computational technique that limits these costly steps to the first iteration. In subsequent iterations, Σ^{-1} and $\det \Sigma$ can be updated by the Sherman-Morrison formula and matrix discriminant lemma.

Notice that in the multivariate setting, the Welford updates and downdates of the sample mean μ and the sample covariance matrix Σ become

$$\begin{aligned}\mu_{h+1} &= \frac{1}{h+1}(h\mu_h + y_{h+1}) \\ \mu_h &= \frac{1}{h}[(h+1)\mu_{h+1} - y_{h+1}] \\ \Sigma_{h+1} &= \frac{h}{h+1}\Sigma_h + \frac{1}{h}(y_{h+1} - \mu_{h+1})(y_{h+1} - \mu_{h+1})^\top \\ \Sigma_h &= \frac{h+1}{h}\Sigma_{h+1} - \frac{h+1}{h^2}(y_{h+1} - \mu_{h+1})(y_{h+1} - \mu_{h+1})^\top.\end{aligned}$$

Given that the update and downdate of Σ are rank-1 perturbations of Σ , we can invoke the Sherman-Morrison formula

$$(A + uv^\top)^{-1} = A^{-1} - \frac{A^{-1}uv^\top A^{-1}}{1 + v^\top A^{-1}u},$$

to update and downdate Σ^{-1} . We can also invoke the the matrix determinant lemma

$$\det(A + uv^\top) = \det(A(1 + v^\top A^{-1}u))$$

to update and downdate $\det \Sigma$.

More specifically, we update Σ_{h+1}^{-1} and $\det \Sigma_{h+1}^{-1}$ via

$$\begin{aligned}\Sigma_{h+1}^{-1} &= \left(\frac{h+1}{h}\Sigma_h^{-1}\right) - \frac{(\frac{h+1}{h}\Sigma_h^{-1})(y_{h+1} - \mu_{h+1})(y_{h+1} - \mu_{h+1})^\top(\frac{h+1}{h}\Sigma_h^{-1})}{h + (y_{h+1} - \mu_{h+1})^\top(\frac{h+1}{h}\Sigma_h^{-1})(y_{h+1} - \mu_{h+1})} \\ \det \Sigma_{h+1} &= \frac{h}{h+1} \det \Sigma_h \left[1 + \frac{1}{h}(y_{h+1} - \mu_{h+1})^\top \left(\frac{h+1}{h}\Sigma_h^{-1}\right) (y_{h+1} - \mu_{h+1})\right].\end{aligned}$$

For the sake of brevity, we omit the similar downdates of Σ_h^{-1} and $\det \Sigma_h^{-1}$. At each concentration step, the new observations inserted into the h -subset are balanced by a like number of deletions of old observations.

B Additional Simulation Results

The following two tables convey simulation results for further overdetermined problems.

Table 3: Simulation results for $(n, p) = (2000, 200)$. All measures are averaged over 50 random replicates. Abbreviations are KL: Kullback–Leibler divergence, FDB: fast depth-based method, and Spec: spectral minimum covariance determinant.

Outlier	Metric	10%		25%		40%	
		FDB	Spec	FDB	Spec	FDB	Spec
Point	e_μ	0.369	0.338	0.389	0.365	56.30	9.748
		(0.015)	(0.009)	(0.014)	(0.016)	(1.944)	(19.71)
	e_Σ	0.663	0.589	0.706	0.650	6.932	1.613
		(0.008)	(0.006)	(0.010)	(0.010)	(0.375)	(1.836)
	KL	14.57	11.65	16.20	14.03	1157	265.2
		(0.258)	(0.156)	(0.225)	(0.132)	(21.15)	(522.0)
Cluster	e_μ	0.372	0.337	0.388	0.360	0.414	0.406
		(0.017)	(0.014)	(0.019)	(0.018)	(0.017)	(0.016)
	e_Σ	0.665	0.589	0.703	0.649	0.756	0.734
		(0.011)	(0.008)	(0.011)	(0.011)	(0.007)	(0.007)
	KL	14.57	11.61	16.14	14.02	18.69	17.80
		(0.191)	(0.100)	(0.203)	(0.152)	(0.180)	(0.141)
Random	e_μ	0.364	0.326	0.386	0.360	0.411	0.401
		(0.019)	(0.014)	(0.014)	(0.013)	(0.030)	(0.031)
	e_Σ	0.661	0.583	0.700	0.647	0.761	0.738
		(0.011)	(0.008)	(0.009)	(0.009)	(0.010)	(0.009)
	KL	14.54	11.61	17.79	16.12	18.67	17.73
		(0.247)	(0.054)	(0.527)	(0.217)	(0.277)	(0.329)
Radial	e_μ	0.371	0.337	0.387	0.360	0.414	0.406
		(0.022)	(0.014)	(0.018)	(0.018)	(0.018)	(0.016)
	e_Σ	0.665	0.587	0.704	0.649	0.756	0.735
		(0.011)	(0.008)	(0.011)	(0.011)	(0.009)	(0.007)
	KL	14.58	11.61	16.22	11.97	18.83	17.80
		(0.247)	(0.010)	(0.199)	(0.304)	(0.185)	(0.141)

References

- Agostinelli, C., Leung, A., Yohai, V. J., and Zamar, R. H. (2015), “Robust estimation of multivariate location and scatter in the presence of cellwise and casewise contamination,” *Test*, 24, 441–461.
- Allison, K. H., Hammond, M. E. H., Dowsett, M., McKernin, S. E., Carey, L. A., Fitzgibbons, P. L., Hayes, D. F., Lakhani, S. R., Chavez-MacGregor, M., Perlmutter, J., Perou, C. M., Regan, M. M., Rimm, D. L., Symmans, W. F., Torlakovic, E. E., Varella, L.,

Table 4: Computation time averaged over 50 random replicates. Abbreviations are FDB: fast depth-based method, and Spec: spectral minimum covariance determinant.

Outlier	Combination	10%		25%		40%	
		FDB	Spec	FDB	Spec	FDB	Spec
Point	(400,40)	0.021	24.19	0.025	23.63	0.022	24.39
	(400,80)	0.092	31.40	0.062	27.79	0.074	31.70
	(2000,200)	2.382	574.1	2.478	607.3	2.391	605.7
Cluster	(400,40)	0.019	23.80	0.019	21.80	0.020	21.95
	(400,80)	0.066	32.60	0.064	29.47	0.073	31.35
	(2000,200)	2.029	521.7	2.128	559.6	1.981	513.6
Random	(400,40)	0.020	26.19	0.021	26.14	0.018	24.28
	(400,80)	0.086	72.74	0.081	59.13	0.069	56.38
	(2000,200)	2.301	1769	2.267	1680	1.929	1474
Radial	(400,40)	0.020	26.42	0.019	24.01	0.022	31.31
	(400,80)	0.068	55.57	0.083	58.18	0.070	57.00
	(2000,200)	2.194	1588	2.400	1751	2.059	1620

Viale, G., Weisberg, T. F., McShane, L. M., and Wolff, A. C. (2020), “Estrogen and Progesterone Receptor Testing in Breast Cancer: ASCO/CAP Guideline Update,” *Journal of Clinical Oncology*, 38, 1346–1366, PMID: 31928404.

Bauer, K. R., Brown, M., Cress, R. D., Parise, C. A., and Caggiano, V. (2007), “Descriptive analysis of estrogen receptor (ER)-negative, progesterone receptor (PR)-negative, and HER2-negative invasive breast cancer, the so-called triple-negative phenotype,” *Cancer*, 109, 1721–1728.

Berenguer-Rico, V., Johansen, S., and Nielsen, B. (2023), “A model where the least trimmed squares estimator is maximum likelihood,” *Journal of the Royal Statistical Society Series B: Statistical Methodology*, 85, 886–912.

Boudt, K., Rousseeuw, P. J., Vanduffel, S., and Verdonck, T. (2020), “The minimum regularized covariance determinant estimator,” *Statistics and Computing*, 30, 113–128.

Butler, R., Davies, P., and Jhun, M. (1993), “Asymptotics for the minimum covariance determinant estimator,” *The Annals of Statistics*, 1385–1400.

Cator, E. A. and Lopuhaä, H. P. (2012), “Central limit theorem and influence function for the MCD estimators at general multivariate distributions,” *Bernoulli*, 18, 520 – 551.

Cerami, E., Gao, J., Dogrusoz, U., Gross, B. E., Sumer, S. O., Aksoy, B. A., Jacobsen, A., Byrne, C. J., Heuer, M. L., Larsson, E., Antipin, Y., Reva, B., Goldberg, A. P.,

- Sander, C., and Schultz, N. (2012), “The cBio Cancer Genomics Portal: An Open Platform for Exploring Multidimensional Cancer Genomics Data,” *Cancer Discovery*, 2, 401–404.
- Cerioni, A. (2010), “Multivariate outlier detection with high-breakdown estimators,” *Journal of the American Statistical Association*, 105, 147–156.
- Fang, Y. and Wang, J. (2012), “Selection of the number of clusters via the bootstrap method,” *Computational Statistics & Data Analysis*, 56, 468–477.
- Filzmoser, P., Maronna, R., and Werner, M. (2008), “Outlier identification in high dimensions,” *Computational statistics & data analysis*, 52, 1694–1711.
- Grübel, R. (1988), “A minimal characterization of the covariance matrix,” *Metrika*, 35, 49–52.
- Hardin, J. and Rocke, D. M. (2005), “The distribution of robust distances,” *Journal of Computational and Graphical Statistics*, 14, 928–946.
- Haslbeck, J. M. and Wulff, D. U. (2020), “Estimating the number of clusters via a corrected clustering instability,” *Computational Statistics*, 35, 1879–1894.
- Hubert, M. and Debruyne, M. (2010), “Minimum covariance determinant,” *Wiley interdisciplinary reviews: Computational statistics*, 2, 36–43.
- Hubert, M., Debruyne, M., and Rousseeuw, P. J. (2018), “Minimum covariance determinant and extensions,” *Wiley Interdisciplinary Reviews: Computational Statistics*, 10, e1421.
- Hubert, M., Rousseeuw, P. J., and Aelst, S. V. (2008), “High-Breakdown Robust Multivariate Methods,” *Statistical Science*, 23, 92 – 119.
- Hubert, M., Rousseeuw, P. J., and Vanden Branden, K. (2005), “ROBPCA: a new approach to robust principal component analysis,” *Technometrics*, 47, 64–79.
- Hubert, M., Rousseeuw, P. J., and Verdonck, T. (2012), “A deterministic algorithm for robust location and scatter,” *Journal of Computational and Graphical Statistics*, 21, 618–637.

- Hubert, M. and Van Driessen, K. (2004), “Fast and robust discriminant analysis,” *Computational Statistics & Data Analysis*, 45, 301–320.
- Lange, K. (2010), *Numerical Analysis for Statisticians*, vol. 1, Springer.
- Lange, T., Mosler, K., and Mozharovskyi, P. (2014), “Fast nonparametric classification based on data depth,” *Statistical Papers*, 55, 49–69.
- Li, C. and Jin, B. (2022), “Outlier Detection via a Block Diagonal Product Estimator,” *Journal of Systems Science and Complexity*, 35, 1929–1943.
- Li, C., Jin, B., and Wu, Y. (2024), “Outlier detection via a minimum ridge covariance determinant estimator,” *Statistica Sinica*, just-accepted.
- Network, T. C. G. A. (2012), “Comprehensive molecular portraits of human breast tumours,” *Nature*, 490, 61–70.
- Pokotylo, O., Mozharovskyi, P., and Dyckerhoff, R. (2016), “Depth and depth-based classification with R-package ddalpha,” *arXiv preprint arXiv:1608.04109*.
- Raymaekers, J. and Rousseeuw, P. J. (2023), “The cellwise minimum covariance determinant estimator,” *Journal of the American Statistical Association*, just-accepted.
- Ro, K., Zou, C., Wang, Z., and Yin, G. (2015), “Outlier detection for high-dimensional data,” *Biometrika*, 102, 589–599.
- Rousseeuw, P. J. (1985), “Multivariate estimation with high breakdown point,” *Mathematical statistics and applications*, 8, 37.
- Rousseeuw, P. J. and Driessen, K. V. (1999), “A fast algorithm for the minimum covariance determinant estimator,” *Technometrics*, 41, 212–223.
- Rousseeuw, P. J. and Leroy, A. M. (2005), *Robust Regression and Outlier Detection*, John Wiley & Sons.
- Schreurs, J., Vranckx, I., Hubert, M., Suykens, J. A., and Rousseeuw, P. J. (2021), “Outlier detection in non-elliptical data by kernel MRCD,” *Statistics and Computing*, 31, 66.
- Sun, W., Wang, J., and Fang, Y. (2013), “Consistent selection of tuning parameters via variable selection stability,” *The Journal of Machine Learning Research*, 14, 3419–3440.

- Tibshirani, R., Walther, G., and Hastie, T. (2001), “Estimating the number of clusters in a data set via the gap statistic,” *Journal of the Royal Statistical Society: Series B (Statistical Methodology)*, 63, 411–423.
- Wang, J. (2010), “Consistent selection of the number of clusters via crossvalidation,” *Biometrika*, 97, 893–904.
- Welford, B. (1962), “Note on a method for calculating corrected sums of squares and products,” *Technometrics*, 4, 419–420.
- Zahariah, S. and Midi, H. (2023), “Minimum regularized covariance determinant and principal component analysis-based method for the identification of high leverage points in high dimensional sparse data,” *Journal of Applied Statistics*, 50, 2817–2835.
- Zhang, M., Song, Y., and Dai, W. (2023), “Fast robust location and scatter estimation: a depth-based method,” *Technometrics*, just-accepted.
- Zuo, Y. (2006), “Multidimensional trimming based on projection depth,” *The Annals of Statistics*, 34, 2211 – 2251.
- Zuo, Y. and Serfling, R. (2000), “General notions of statistical depth function,” *The Annals of Statistics*, 461–482.